Chemistry Europe
European Chemical Societies Publishing

Special Collection

A Dimethylaminophenyl-Substituted Naphtho[1,2-*b*]quinolizinium as a Multicolor NIR Probe for the Fluorimetric Detection of Intracellular Nucleic Acids and Proteins

Peter Jonas Wickhorst,[a] Sergey I. Druzhinin,[a] Heiko Ihmels,*[a] Mareike Müller,[a] Manlio Sutera Sardo,[b] Holger Schönherr,[a] and Giampietro Viola[c]

This paper is dedicated to Prof. Dr. Michael Schmittel on the occasion of his 65th birthday.

The dye 3-(4-(*N*,*N*-dimethylamino)phenyl)naphtho[*1,2-b*]quinolizinium was synthesized by means of a Suzuki–Miyaura reaction in good yield, and its binding properties with duplex DNA, quadruplex DNA (G4-DNA), RNA, and bovine serum albumin (BSA) were investigated by photometric, fluorimetric and polarimetric titrations and DNA denaturation analysis. The compound intercalates into DNA and RNA, associates in binding site I of BSA, and binds to G4-DNA by terminal π stacking. The ligand exhibits a fluorescence light-up effect upon complexation to these biomacromolecules, which is more pronounced and blue shifted in the presence of BSA ($\Phi_{fl} = 0.29$, $\lambda_{fl} = 627$ nm) than with the nucleic acids ($\Phi_{fl} = 0.01$–0.05, $\lambda_{fl} = 725$–750 nm). Furthermore, the triple-exponential fluorescence decay of the probe when bound to biomacromolecules in a cell enables their visualization in this medium and the differential labeling of cellular components.

1. Introduction

The detection of biological relevant analytes with fluorescent dye molecules has developed into a useful method for live cell imaging and is used for the visualization of various bioanalytes in living organisms[1] In this context, organic probe molecules that change their emission properties when they are bound to a receptor or host molecule have been utilized successfully for the selective fluorimetric detection of specific analytes.[1] However, many of these fluorescent probes operate in a wavelength region (400–700 nm), which is disadvantageous for an application in biological systems due to the background fluorescence in this wavelength region and strong light scattering.[2,3] Hence, fluorescent dyes that emit in the near infrared region (NIR; >700 nm) have gained much interest in bioanalytical chemistry, because their emission is not hampered by the intrinsic autofluorescence of cells, and the applied excitation light as well as the emission penetrate deeper through biological tissue and cells.[2,3] As a result, such fluorescent NIR probes have been utilized for the detection of various biomolecules such as DNA,[4–10] RNA,[10,11] or proteins.[5,12] Furthermore, the selective detection of biologically relevant non-canonical DNA structures like G-quadruplex DNA (G4-DNA) was achieved with fluorescent NIR probes.[4–8] Along these lines, many so-called light-up probes based on, for example, carbazole,[13] coralyne,[14] cyanine,[15] pyridinium,[7] quinolinium,[10,16] and squaraine[17] derivatives have been developed that exhibit a strong increase of their emission intensity upon binding to biologically relevant molecules.

In this context, we and others have introduced and utilized the quinolizinium cation as starting point for the development for the fluorimetric detection of biomolecules.[4,5,18] But although several annelated quinolizinium derivatives have been investigated already in detail as tools for fluorimetric detection, the naphtho[1,2-*b*]quinolizinium (**1**) has not been functionalized as fluorescent light-up probe, yet, even though the parent compound **1** exhibits the required properties of a DNA-sensitive fluorescent probe. Namely, it exhibits high binding affinity to DNA[19,20] and favorable photophysical properties, such as reasonable emission quantum yield of the parent compound. Moreover, a strong fluorosolvatochromism has been observed with aryl-substituted derivatives **2a–d** (Figure 1).[21,22] However, to be used as fluorescent light-up probe

[a] *P. J. Wickhorst, Dr. S. I. Druzhinin, Prof. Dr. H. Ihmels, Dr. M. Müller, Prof. Dr. H. Schönherr*
Department of Chemistry – Biology
University of Siegen, and
Center of Micro- and Nanochemistry and (Bio)Technology (Cμ)
Adolf-Reichwein-Str. 2, 57068 Siegen (Germany)
E-mail: ihmels@chemie.uni-siegen.de
[b] *Dr. M. Sutera Sardo*
Department of Pharmaceutical Sciences
via Marzolo 5, 35131 Padova (Italy)
[c] *Prof. Dr. G. Viola*
Department of Women's and Child's health,
Oncohematology laboratory
University of Padova
Via Giustiniani 2, I-35128 Padova (Italy)

Supporting information for this article is available on the WWW under https://doi.org/10.1002/cptc.202100148

Special Collection An invited contribution to the "GDCh and ChemPhotoChem: 5-Year Anniversary" Special Collection.

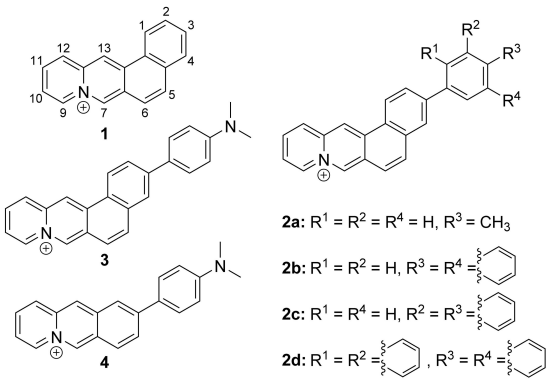

Figure 1. Structure of naphtho[1,2-*b*]quinolizinium derivatives **1**–**3** and 9-(4-*N*,*N*-dimethylaminophenyl)benzo[*b*]quinolizinium (**4**).

the emission of the naphtho[1,2-*b*]quinolizinium has to be initially quenched and only released on binding to the target analyte. In addition, the emission has to be red shifted for an application as a NIR probe. We proposed that both properties may be accomplished by the attachment of a dimethylaminophenyl substituent because this approach has already been successfully applied to the benzo[*b*]quinizinium fluorophore.[5] In fact, the fluorescence of the corresponding 9-(4-dimethylaminophenyl)benzo[*b*]quinolizinium (**4**) is efficiently quenched by a combination of torsional relaxation and a charge shift (CS) in the excited molecule.[5] In turn, these processes are suppressed when the molecule is bound to biomacromolecules, such as DNA and BSA, which leads to a distinct increase of its emission quantum yield. Moreover, the absorption and emission of derivative **4** are strongly red shifted in the presence of DNA, even slightly in the NIR range, as compared with that of the parent compound. This strong red shift is likely the result of the donor-acceptor interplay between the aniline moiety and the benzoquinolizinium unit. Based on these observations, we concluded that an aminophenyl-substituted naphthoquinolizinium derivative may exhibit similar beneficial photophysical properties along with an enhanced affinity towards DNA. Hence, we functionalized the naphtho-[1,2-*b*]quinolizinium with a dimethylaminophenyl substituent and investigated its emission properties upon binding to different biomolecules as well as its application for cell imaging.

2. Results and Discussion

2.1. Synthesis

The target compound 3-(4-*N*,*N*-dimethylaminophenyl)naphtho-[1,2-*b*]quinoliziniumbromide (**3**) was synthesized in 72% yield with a Suzuki-Miyaura coupling reaction of 3-bromonaphtho-[1,2-*b*]quinolizinium (**5**)[22] and 4-*N*,*N*-dimethylaminophenylboronic acid (**6**) with Pd(dppf)$Cl_2 \cdot CH_2Cl_2$ as catalyst (Scheme 1).[22,23] The structure of the product **3** was confirmed by NMR-spectroscopic analysis (^{1}H, ^{13}C, COSY, HSQC, HMBC),[24] elemental analysis and mass-spectrometric data. Specifically,

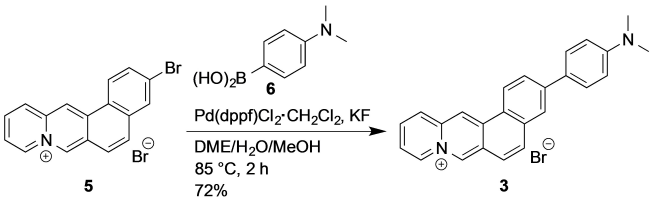

Scheme 1. Synthesis of 3-(4-*N*,*N*-dimethylaminophenyl)naphtho[1,2-*b*]-quinoliziniumbromide (**3**).

the downfield-shifted ^{1}H-NMR signals of the protons 7-H and 13-H at 10.19 ppm and 9.95 ppm indicated the integrity of the naphthoquinolizinium unit (cf. SI: Figure S13). Moreover, clear HMBC cross-peaks between C3 of the naphthoquinolizinium unit and 2′-H and 6′-H of the aniline substituent unambiguously confirmed the formation of the product **3** (cf. SI: Figure S15).

2.2. Absorption and Emission Properties

The absorption of the naphthoquinolizinium derivative **3** changed in different solvents with long-wavelength absorption maxima between 413 nm in aqueous buffer and 457 nm in $CHCl_3$ (Table 1, cf. SI: Figure S1A,B). Likewise, the emission properties of compound **3** depend strongly on the solvent. Thus, while **3** is essentially non-fluorescent in the polar solvents water, MeOH, MeCN, and DMSO, a very weak fluorescence was detected in EtOH ($\Phi_{fl} = 0.01$) and 1-PrOH ($\Phi_{fl} = 0.02$). In contrast, a significantly larger emission quantum yield was determined in $CHCl_3$ solution ($\Phi_{fl} = 0.11$). Furthermore, the emission maxima, if detectable, were markedly red shifted in polar protic solvents EtOH ($\lambda_{fl} = 762$ nm) and 1-PrOH ($\lambda_{fl} = 750$ nm) as compared with the one in $CHCl_3$ ($\lambda_{fl} = 627$ nm). The emission properties were also studied in media with higher viscosity to examine whether the low emission quantum yields of compound **3** result from conformational changes in the excited state.[25] For that purpose, the fluorescence spectra of **3** were recorded in glycerol solutions at varying temperatures (Figure 2, cf. SI: Figure S1D). It was observed that the fluorescence of **3** was significantly quenched at higher temperature and lower viscosity (e.g. $\Phi_{fl} = 0.02$, 80 °C, $\eta = 32$ cP)[26] as

Table 1. Absorption and emission properties of derivative **3** in different solvents.

Solvent	λ_{abs}[a] [nm]	log ε[b]	λ_{fl}[c] [nm]	Φ_{fl}[e]
H_2O	413	4.22	[d]	[d]
MeOH	425	4.34	[d]	[d]
EtOH	440	4.32	762	0.01
1-PrOH	444	4.31	750	0.02
MeCN	424	4.36	[d]	[d]
DMSO	426	4.32	[d]	[d]
$CHCl_3$	457	4.37	627	0.11

[a] Long-wavelength absorption maximum; $c = 20$ μM. [b] ε = Molar extinction coefficient in $cm^{-1}M^{-1}$. [c] Fluorescence maximum at $\lambda_{ex} = 425$ nm. [d] Fluorescence quantum yield too low to be determined. [e] Fluorescence quantum yield relative to rhodamine B in EtOH ($\Phi_{fl} = 0.66$).[28]

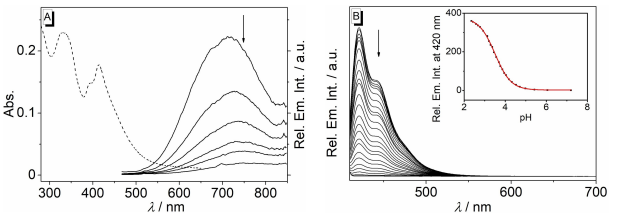

Figure 2. A: Absorption spectra (dashed line) of **3** ($c = 10$ μM, with 5% v/v DMSO) in BPE (biphosphate EDTA) buffer and emission spectra (continuous lines) of **3** ($c = 10$ μM, with 0.25% v/v DMSO) in glycerol at 20 °C, 30 °C, 40 °C, 50 °C, 60 °C, and 80 °C; $\lambda_{ex} = 450$ nm. The arrows indicate the changes of the emission intensity with increasing temperature. B: Fluorimetric titration of aqueous NaOH solution (2 M) to a solution of **3** ($c = 20$ μM) in Britton–Robinson buffer; $\lambda_{ex} = 405$ nm. The arrows indicate the development of emission bands with increasing pH values. Inset: Plot of the emission intensity at 420 nm *versus* pH of the solution. The red line indicates the fit of the experimental data to the theoretical titration curve of a weak acid.

compared with the glycerol solution at 20 °C that has a much higher viscosity ($\Phi_{fl} = 0.18$, $\eta = 1400$ cP).

Additionally, the dependence of the absorption and emission properties of **3** on the pH of the medium was studied (Figure 2, cf. SI: Figure S1C). Notably, at pH 2 derivative **3** exhibits strongly blue-shifted absorption bands at 408 nm, 387 nm and 325 nm and an intense emission band at 420 nm ($\Phi_{fl} = 0.06$). With increasing pH of the solution, a broad red-shifted absorption band at 413 nm developed, whereas the emission band was steadily quenched. The analysis of the titration curve obtained from the fluorimetric acid-base titration revealed a pK_a of 3.50 ± 0.01 (cf. SI).[27]

2.3. Photometric Titrations with Biomacromolecules

The changes of the absorption properties of compound **3** upon binding to different biologically relevant macromolecules were followed by photometric titrations (Figure 3, cf. SI: Figure S2). For this purpose, different nucleic acids were selected, such as calf thymus (ct) DNA, the quadruplex-forming oligonucleotides d[A(TTAGGG)$_3$GGG] (**22AG**),[29] d[(ACAGGGTGT)$_2$] (**a2**),[30] d[TGA(G$_3$TG$_3$TA)$_2$] (**c–myc**)[31] and d[AG$_3$AG$_3$CGCTG$_3$AG$_2$AG$_3$] (**c–kit**),[32] as well as torula yeast (ty) RNA. In addition, bovine serum albumin (BSA) was chosen as representative protein. Upon addition of the nucleic acids and BSA a decrease of the absorption bands at 414 nm and 330 nm was observed in each case, which was accompanied by the development of new red-shifted absorption maxima. Interestingly, the latter effect was significantly more pronounced for complexes with the nucleic acids ($\Delta\lambda = 13$–22 nm) as compared with that in the presence of BSA ($\Delta\lambda = 5$ nm). Moreover, the hypochromic effect was much more pronounced for complexes with RNA (log $\varepsilon = 3.93$) as compared with those of the other tested biomolecules (log $\varepsilon = 4.14$–4.21). Notably, no isosbestic points were observed during the photometric titrations of ligand **3**.

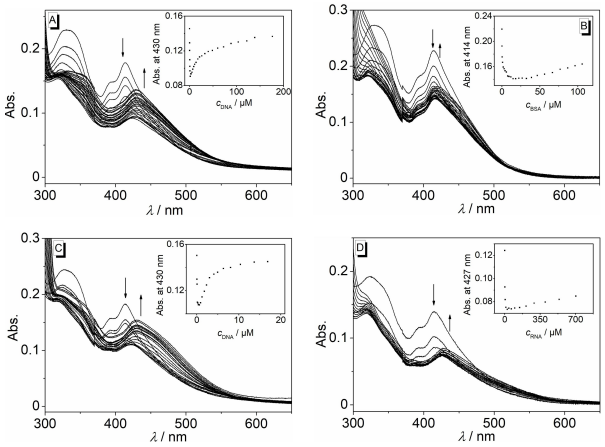

Figure 3. Photometric titration of **3** ($c = 10$ μM) with ct DNA (A) and BSA (B) in BPE buffer ($c_{Na+} = 16$ mM, pH 7.0, with 10% v/v DMSO), with **22AG** (C) in K-phosphate buffer ($c_{K+} = 110$ mM, pH 7.0, with 10% v/v DMSO) and with ty RNA (D) in TBS (tris-buffered saline) buffer ($c_{Na+} = 150$ mM, pH 7.0, with 10% v/v DMSO). The arrows indicate the changes of absorption upon addition of DNA, BSA and RNA, respectively. Inset: Plot of the ligand absorption *versus* DNA concentration.

2.4. CD and LD Spectroscopy

The association of ligand **3** with ct DNA, **22AG**, **a2**, **c-myc**, **c-kit** and ty RNA was additionally followed by circular dichroism (CD) and *flow* linear dichroism (LD) spectroscopy (Figure 4, cf. SI: Figure S8). Upon addition of the ligand to ct DNA, a continuous development of negative induced CD (ICD) and LD signals at the absorption maxima at 450 nm and 335 nm was observed. Moreover, the CD signals of ct DNA at 258 nm and 278 nm continuously decreased with increasing ligand content. Notably, a similar ICD pattern was observed during the titration of ty RNA with ligand **3** (cf. SI: Figure S8C). In the presence of ligand **3** the quadruplex-forming oligonucleotides **a2**, **c-myc** and **c-kit** did not induce meaningful changes of the CD spectra.

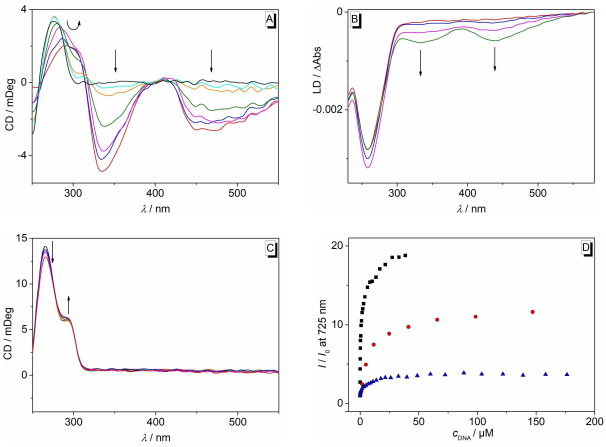

Figure 4. CD spectra (A,C,D) and LD spectra (B) of ct DNA (A,B, $c_{DNA} = 20$ μM), **a2** (C, $c_{DNA} = 20$ μM) and **22AG** (D, $c_{DNA} = 20$ μM) in the absence and presence of **3** [*LDR* = 0 (black), 0.05 (cyan), 0.2 (orange), 0.5 (green), 1.0 (magenta), 1.5 (blue), 2.0 (red)] in BPE buffer solution (10 mM, pH 7.0; with 5% v/v DMSO). The arrows indicate the changes of absorption upon addition of DNA.

In contrast, during the titrations with **22AG** a decrease of the shoulder at 255 nm alongside with an increase of the CD signal at 290 nm were observed. Nevertheless, no ICD signals of the ligand developed during the titrations with **22AG**, **a2**, **c-myc** and **c-kit**.

2.5. Thermal DNA Denaturation Experiments

The influence of ligand **3** on the thermal stability of G4-DNA was further tested by thermal DNA-denaturation experiments with dye-labeled, quadruplex-forming oligonucleotides **F21T**, **Fa2T**, **FmycT**, and **FkitT** (Table 2, cf. SI: Figure S6, Figure S7).[33] Derivative **3** induced a significant increase of the melting temperature, ΔT_m, of all tested oligonucleotides. However, while **F21T** ($\Delta T_m = 10.0\,^{\circ}C$, at *LDR* = 5), **FkitT** ($\Delta T_m = 6.7\,^{\circ}C$) and **FmycT** ($\Delta T_m = 5.6\,^{\circ}C$) exhibited a relative strong shift of their melting temperature in the presence of the ligand, **Fa2T** ($\Delta T_m = 3.0\,^{\circ}C$) was only stabilized weakly. Furthermore, the shifts of melting temperature of **F21T**, **Fa2T** and **FmycT** were only affected marginally by the presence of the duplex DNA-forming oligonucleotide **ds26** (**F21T/ds26**: $\Delta\Delta T_m = 1.0\,^{\circ}C$; **FmycT/ds26**: $\Delta\Delta T_m = 1.3\,^{\circ}C$; **Fa2T/ds26**: $\Delta\Delta T_m = 0.3\,^{\circ}C$, cf. SI: eq. 4). The quadruplex **FkitT**, however, exhibited a significant shift of its ΔT_m values in the presence of duplex DNA (**FkitT/ds26**: $\Delta\Delta T_m = 2.4\,^{\circ}C$).

2.6. Fluorescent Indicator Displacement Experiments with BSA

The binding of ligand **3** to BSA was further studied by fluorimetric displacement experiments with the known BSA-binding ligands dansylamide (DNSA) and dansyl-*L*-proline (DP) that bind selectively to binding site I (DNSA) or binding site II (DP) of the protein (Figure S5). In this fluorescent indicator displacement (FID) assay, the binding of the analyte to the respective binding site is indirectly monitored by the changes of the fluorescence of the displaced ligand.[34] In the case of compound **3**, the addition of DNSA to a mixture of **3** and BSA resulted in a significant quenching of the fluorescence, whereas no significant changes of the fluorescence were observed during the titration with DP.

Table 2. Binding constants K_b and shifts of melting temperature ΔT_m of **3** with duplex and G4-DNA, and fluorescence quantum yields of the DNA-bound ligands.

	K_b [M^{-1}][b]	Φ_{fl} [c]	ΔT_m [°C][d]	$\Delta\Delta T_m$ [°C][e]
ct DNA	$4.9 \pm 0.6 \times 10^4$	0.01	–	
22AG/F21T[a]	$2.6 \pm 0.4 \times 10^5$	0.05	10.0	1.0
c-kit/FkitT [a]	$4.4 \pm 0.7 \times 10^5$	0.03	6.7	2.4
a2/Fa2T[a]	$3.9 \pm 0.5 \times 10^5$	0.05	3.0	0.3
c-myc/FmycT[a]	$3.9 \pm 0.7 \times 10^5$	0.03	5.6	1.3
ty RNA	$1.5 \pm 0.3 \times 10^5$	0.03	–	
BSA	$8.9 \pm 0.5 \times 10^3$	0.29	–	

[a] Dye-labeled oligonucleotides: **F21T** = fluo-$G_3(TTAG_3)_3$-tamra, **Fa2T** = fluo-$(ACAG_3TGT)_2$-tamra, **FmycT** = fluo-$TGAG_3TG_3TAG_3TG_3TA$-tamra, **FkitT** = fluo-$AG_3AG_3CGCTG_3AG_2AG_3$-tamra, fluo = fluorescein, tamra = tetramethylrhodamine. [b] Determined from fluorimetric titrations (cf. Figure S4). [c] Fluorescence quantum yield relative to rhodamine B in EtOH ($\Phi_{fl} = 0.66$).[28] [d] Determined from fluorimetric analysis of dye-labeled oligonucleotides, *LDR* = 5; $c_{DNA} = 0.2$ μM (in oligonucleotides); KCl–LiCl-cacodylat buffer $c_{K+} = 10$ mM, $c_{Na+} = 10$ mM, $c_{Li+} = 90$ mM, pH 7.0), $\lambda_{ex} = 470$ nm; $\lambda_{em} = 515$ nm; estimated error: ±0.5 °C. [e] Difference between the melting temperature of dye labeled oligonucleotides with and without oligonucleotide **ds26**, *LDR* = 5; $c_{G4\text{-}DNA} = 0.2$ μM (in oligonucleotides); $c_{ds26} = 3.0$ μM (in oligonucleotides); KCl–LiCl-cacodylat buffer $c_{K+} = 10$ mM, $c_{Na+} = 10$ mM, $c_{Li+} = 90$ mM, pH 7.0) $\lambda_{ex} = 470$ nm; $\lambda_{em} = 515$ nm; estimated error: ±0.5 °C.

2.7. Fluorimetric Titrations with Biological Host Molecules

The association of ligand **3** with ct DNA, **22AG**, **a2**, **c-myc**, **c-kit**, ty RNA, and BSA was followed by fluorimetric titrations (Figure 5, Figure 6, cf. SI: Figure S3). The essentially non-fluorescent ligand developed relatively strong emission bands upon addition of all tested biomolecules. Hence, upon addition of DNA and RNA distinct emission bands at 725–750 nm were formed, whereas a blue-shifted emission at 627 nm was observed during the titration with BSA. Moreover, the emission

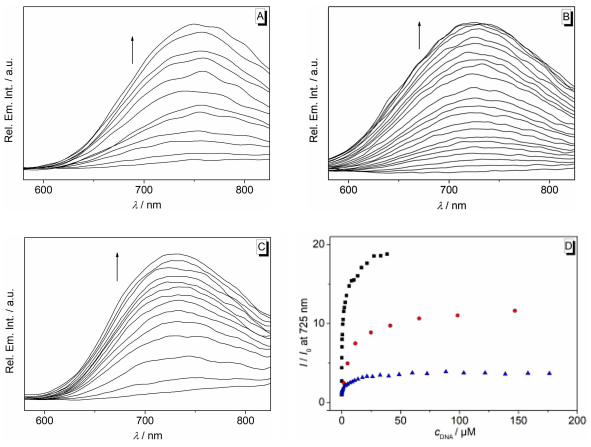

Figure 5. Fluorimetric titration of **3** ($c = 10$ μM) with ct DNA (A) in BPE buffer ($c_{Na+} = 16$ mM, pH 7.0, with 10% v/v DMSO), with **22AG** (B) in K-phosphate buffer ($c_{K+} = 110$ mM, pH 7.0, with 10% v/v DMSO) and with ty RNA (C) in TBS buffer ($c_{Na+} = 150$ mM, pH 7.0, with 10% v/v DMSO); $\lambda_{ex} = 450$ nm. The arrows indicate the changes of absorption upon addition of DNA. Relative changes of the emission intensity of **3** (D) upon addition of ct DNA (blue triangles), **22AG** (black squares) and ty RNA (red circles).

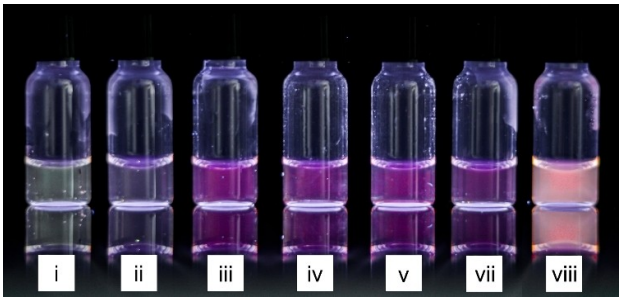

Figure 6. Pictures of the emission color of **3** ($c = 20$ μM) in BPE buffer (i) and in the presence of one equivalent ct DNA (ii), **22AG** (iii), **a2** (iv), **c-kit** (v), and **c-myc** (vi), ty RNA (vii), BSA (viii); $\lambda_{ex} = 366$ nm.

intensity of the bound ligand depends strongly on the employed host molecule. Thus, complexes with **22AG** and **a2** exhibited slightly stronger fluorescence bands ($\Phi_{fl}=0.05$) as compared with the ones of complexes with ct DNA ($\Phi_{fl}=0.01$), ty RNA ($\Phi_{fl}=0.03$), **c–myc** ($\Phi_{fl}=0.01$) and **c-kit** ($\Phi_{fl}=0.01$). Most notably, the emission in the presence of BSA was strongly blue shifted, and the light-up effect was also significantly stronger ($\Phi_{fl}=0.29$) as compared with that of all other tested biomacromolecules. The binding isotherms obtained from the spectrofluorimetric titrations were fitted to a theoretical model to obtain the binding constants K_b of ligand **3** (Table 2, cf. SI: Figure S4).[35] Thus, ligand **3** has a high affinity to all tested nucleic acids ($K_b=1.5-4.4\times10^5$ M^{-1}) and a comparatively weak affinity to BSA ($K_b=8.9\times10^3$ M^{-1}).

2.8. Fluorimetric Analysis of Cells

Finally, the ability of dye **3** to stain biomacromolecules was studied in eukaryotic cells. For this purpose, epi fluorescence and confocal fluorescence images of NIH 3T3 mouse fibroblasts[36] were recorded after fixation of the cells and subsequent incubation with a solution of ligand **3** for 1 h (Figure 7, Figure S9, Figure S10, Figure S11). Interestingly, a blue, green and red emission was detected in the cytoplasm of the cells after staining with ligand **3**, whereas no emission in the nucleus was detected. It was found that incubation of the cells in the ligand solution and subsequent fixation of the cells did not result in any detectable staining of the cells' nuclei and in a much lower emission intensity in the cytoplasm (Figure S10), as can be detected with a conventional epifluorescence microscope.

The details of the NIH 3T3 mouse fibroblast staining were also investigated with a more sensitive confocal fluorescence microscope. With the same sample (Figure 7) stained by **3**, the cytoplasm and the nuclei showed 750 and 530 times higher fluorescence intensity per unit area (Figure S12B–D) compared with the intensity of the autofluorescence of NIH 3T3 cells in comparable regions (Figure S12A). Fluorescence of **3** decays in these areas triple-exponentially with the same lifetimes $\tau=9.7$, 3.6 and 1.2 ns, but with different contributions F (Table S1). A substantially higher contribution (2.1 times) was observed in the nucleus for the component with the longest lifetime $\tau=$ 9.7 ns. As in this case the averaged decay times $<\tau>$ become larger in the nucleus region, it allows mapping of the cells (Figure 8) at high contrast with fluorescence lifetime imaging microscopy (FLIM). Here, the nuclei are depicted in red (the longest $<\tau>$), the cytoplasm in green and yellow (moderate $<\tau>$) and background in blue (shortest $<\tau>$). Some regions within the nucleus were found to exhibit shorter lifetimes $<\tau>$ than the rest of the nucleus.

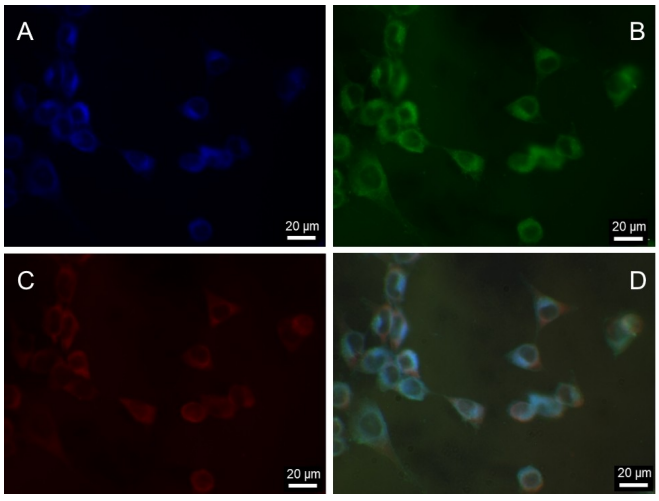

Figure 7. Epifluorescence microscopy images of fixed NIH 3T3 mouse fibroblasts after incubation with **3** (5 µM) in PBS for 1 h. A: $\lambda_{ex}=320$–390 nm, $\lambda_{em}=420$–470 nm; B: $\lambda_{ex}=450$–490 nm, $\lambda_{em}>515$ nm; C: $\lambda_{ex}=540$–552 nm, $\lambda_{em}>590$ nm; D: overlay of all pictures A–C with bright field microscopy picture. Scale bars: 20 µm.

3. Discussion

3.1. Absorption and Emission Properties

As compared with the absorption and emission of the phenyl-substituted naphtho[1,2-*b*]quinolizinium derivative **1a**[22] the long-wavelength absorption maximum and emission maximum of derivative **3** is strongly red shifted (e.g. in $CHCl_3$: $\Delta\lambda_{abs}=$ 43 nm; $\Delta\nu_{abs}=2270$ cm^{-1}, $\Delta\lambda_{fl}=199$ nm; $\Delta\nu_{fl}=7420$ cm^{-1}). This effect was already observed for derivative **4** and is likely the result of the pronounced donor-acceptor interplay between the electron-donating aminophenyl substituent and the annelated quinolizinium ion.[23] Furthermore, the derivative **3** exhibits a blue-shifted emission in nonpolar solvents, namely in $CHCl_3$, as compared with that in polar protic solvents EtOH and 1-PrOH, which may be interpreted as a result of a CS from the dimethylaminophenyl substituent to the quinolizinium in the excited state (Scheme 2).[37,38] Thus, the red-shifted emission in polar solvents is caused by a more efficient stabilization of the excited CS state in these polar media. However, this assumption could not be supported by a more extensive investigation of

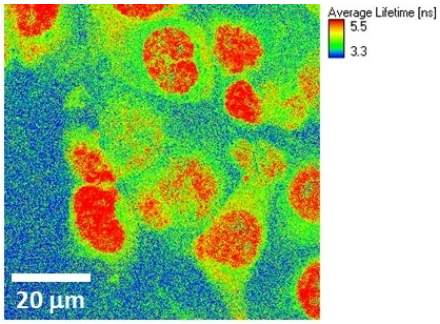

Figure 8. FLIM image mapping the averaged fluorescence decay time $<\tau>$ calculated for each pixel of Figure S12B of NIH 3T3 mouse fibroblasts after incubation with **3** (5 µM) for 1 h by fluorescence decay analysis; $\lambda_{ex}=485$ nm, $\lambda_{em}>520$ nm. The scale represents 20 µm. Blue (red) color corresponds to $<\tau><3.3$ (>5.5) ns, respectively. The same sample as the one shown in Figure 7 was analyzed.

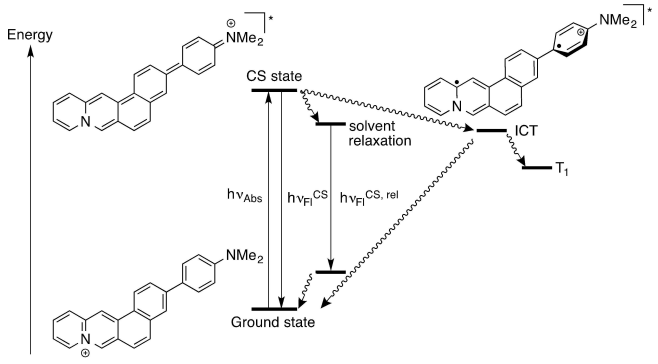

Scheme 2. Charge shift (CS) state and formation of a non-radiative ICT state upon excitation of derivative **3**.

the fluorosolvatochromism of derivative **3** because of its low solubility and its very low emission quantum yields in most organic solvents.

Presumably, the low fluorescence quantum yields of **3** in polar solvents are caused also by the CS process or by an intramolecular charge transfer (ICT). In particular, ICT states of both planar and strongly twisted amino-substituted donor-acceptor fluorophores often possess a much lower fluorescence quantum yield and a lower radiative rate constant.[39] And these excited ICT states, and presumably CS states as well, are mainly deactivated by a non-radiative intersystem crossing (ISC) to a triplet state. Likewise, it was suggested that excitation of aminophenyl-substituted pyridinium derivatives leads to the non-radiative twisted ICT state (TICT).[40] Since the excited ICT state is highly polar, its formation is favored in polar media, which in turn leads to lower fluorescence quantum yields in these solvents. This assumption was further supported by the observed strong increase of the emission intensity in viscous media at lower temperatures. In general, the torsional relaxation of excited biaryl derivatives is slowed down in viscous media which also affects their emission properties.[41] In this particular case, the CS-TICT transition requires a rotation about the biaryl axis, which is slowed down in more viscous media, resulting in an increased fluorescence quantum yield from the CS state.[37] Additionally, the solvation of the CS state in viscous polar media is slowed down[39a,42] preventing an efficient non-radiative deactivation of the ICT states with low energy. Lastly, the increased emission intensity of compound **3** in acidic solution is caused by the complete suppression of the photoinduced CS by protonation of the aniline substituent, so that the regular and fairly emissive excited state of the quinolizinium unit is reached, as has been already observed for the resembling derivative **4**.[23,43]

3.2. Association with DNA and RNA

In general, the decrease and red shifts of the absorbance of ligand **3** upon addition of DNA or RNA clearly prove its association with these host molecules. Nevertheless, the absence of isosbestic points during the photometric titrations reveals the formation of more than two absorbing species during the titration and thus indicates several binding modes at different ligand-host ratios. In addition to the results from photometric titrations, the association of **3** with G4-DNA was confirmed by the increased T_m values of the oligonucleotides upon addition of the ligand. Notably, only a small shift of melting temperature was observed for **Fa2T** ($\Delta T_m = 3.0\,^{\circ}C$) in the presence of **3**, indicating a relatively weak stabilization of the quadruplex towards thermally induced unfolding by the ligand. Nevertheless, a weak stabilization of **Fa2T** was also observed with several ligands that otherwise exhibit a strong binding affinity to this oligonucleotide.[44] And it has been proposed already that the discrepancy between the low ΔT_m values and the relatively high binding constants may originate from the different affinity of a ligand at different temperatures and the intricate, temperature-dependent equilibrium between different quadruplex forms of this oligonucleotide.[44] Most notably, the DNA melting analysis revealed a highly selective stabilization of most employed G4-DNA structures in competition with duplex DNA, as shown by the small changes of ΔT_m values of the G4-DNA **F21T**, **Fa2T** and **FmycT** in the presence of the ligand and duplex DNA **ds26**. As the only exception, the presence of duplex DNA had a more pronounced effect on the ligand-induced melting temperature of **FkitT** (**FkitT**-**ds26**: $\Delta\Delta T_m = 2.4\,^{\circ}C$) which may be the result of a less selective binding towards this quadruplex. The selectivity of ligand **3** towards G4-DNA was also reflected in the larger binding constants with this DNA form ($K_b = 2.6-4.4\times10^5\ M^{-1}$) as compared with the ones with ct DNA ($K_b = 4.9\times10^4\ M^{-1}$) and ty RNA ($K_b = 1.5\times10^5\ M^{-1}$). Notably, the ligand exhibits significantly higher binding constants towards all DNA forms than the structurally related ligand **4** ($K_b = 1.3-8.3\times10^4\ M^{-1}$)[5] which may be the result of a larger π overlap between ligand and DNA bases due to the more extended aromatic π system of the naphthoquinolizinium. The latter assumption is supported by a similar difference of binding constants of duplex DNA with the corresponding parent compound **1** ($K_b = 1.9\times10^5\ M^{-1}$)[20] and the benzo[*b*]quinolizinium ($K_b = 1.2\times10^4\ M^{-1}$).[19]

The negative ICD and LD signals of the ligand in the presence of ct DNA clearly prove its intercalative binding mode, because a negative ICD signal results from a transition moment of the ligand orientated parallel to the long axis of the DNA bases, and a negative LD signal indicates a coplanar orientation of the ligand relative to the DNA bases.[45–47] Moreover, the decrease of the CD signals of ct DNA at 258 nm and 278 nm may result from an overlapping ICD signal of the ligand or the partial unwinding of the helix, which is usually also related to an intercalation of the ligand into the DNA.[45,46] These results are in good agreement with the already reported intercalative binding mode of the parent naphtho[1,2-*b*]-quinolizinium.[20] Interestingly, a similar ICD pattern was observed during the titration of ty RNA with ligand **3** (cf. SI: Figure S8C). In analogy, the ICD signals of the RNA-bound ligand originate from a transition moment of the ligand orientated parallel to the long axis of the RNA bases, which may indicate a binding mode by terminal stacking or intercalation into local double-helical structures of the RNA.[46]

However, due to the undefined content of the employed ty RNA the binding mode of the ligand to this RNA cannot be determined unambiguously. Nevertheless, the weak changes of the RNA signal itself at 290 nm suggests that no significant ligand-induced changes of the RNA structure occur, which has been observed also for other RNA-binding molecules.[48]

The CD signature of the G4-DNA forms **a2**, **c-myc** and **c-kit** changed only marginally upon addition of the ligand **3**, which indicates that the ligand does not influence the structure of these quadruplexes.[49] Nevertheless, addition of ligand **3** to **22AG** led to a decrease of the shoulder at 255 nm alongside with the increase of the CD signal at 290 nm. Since this signal at 255 nm is related to the hybrid-type [3 + 1] conformer and the signal at 290 nm belongs to the basket-type quadruplex conformation, the changes in the CD pattern point to a shift of the equilibrium between these forms in favor of the basket-type structure.[50] Lastly, no ICD signals of the ligand were observed during titrations with G4-DNA and triplex DNA. Since a groove-bound ligand usually exhibits a positive ICD signal[47,51] the absence of ICDs is interpreted as a result of a binding mode by terminal stacking to G4-DNA,[51,52] which is, however, a speculative interpretation because it is based exclusively on the absence of signals.

The fluorimetric titrations revealed a significant light-up effect upon complexation of ligand **3** to all tested nucleic acids. Since the initially low fluorescence intensity of this compound is mainly caused by the formation of a non-radiative CS or ICT state (see above), the increased emission intensity upon binding to the host molecules is likely caused by a suppression of this deactivation channel of the molecule. In this context, two factors that influence the formation of the CS or ICT state need to be considered. Firstly, conformational changes of the excited ligand are hindered due to the steric constraints in the binding site, which prevents the formation of the ICT state by, for instance, a suppression of the rotational degrees of freedom of the ligand. Secondly, the formation of the more polar CS or ICT state is less favorable due to the low polarity of the binding pockets,[53] thus also causing higher fluorescence quantum yields. Most notably, the emission properties of **3** in the presence of the different G4-DNA structures depend on the particular quadruplex form. Thus, while a more pronounced fluorescence was observed in the presence of parallel/antiparallel G4-DNA **a2** ($\Phi_{fl} = 0.05$) and the hybrid-type antiparallel-parallel structure of **22AG** ($\Phi_{fl} = 0.05$), the parallel G4-DNA structures **c-myc** ($\Phi_{fl} = 0.01$) and **c-kit** ($\Phi_{fl} = 0.01$) did not exhibit such a strong light-up effect, which may be caused by the different loop structures of the quadruplexes. Hence, G4-DNA **a2** and **22AG** exhibit loops above the terminal quartet[54] which may cause a tighter accommodation of the ligand in these binding sites. In contrast, **c-myc** and **c-kit** do not exhibit such a loop structure due to their parallel conformation,[55] which enables higher flexibility of the ligand and, in turn, results in a weaker fluorescence. Finally, the emission of the complexes of **3** with ct DNA ($\Phi_{fl} = 0.01$) and ty RNA ($\Phi_{fl} = 0.03$) were slightly less intense as compared with the complexes with **22AG** and **a2**, which is presumably caused by the intercalation of the ligand to duplex DNA and RNA. In this particular binding mode, the relatively large naphthoquinolizinium unit only occupies the intercalation site partially[56] such that the aminophenyl substituent is already located significantly outside the binding site, thus enabling more conformational flexibility.

3.3. Association with BSA

The binding of ligand **3** with BSA was indicated by the decrease and red shift of its absorption bands upon addition of the protein. However, the binding affinity was significantly lower as compared with the ones of the tested nucleic acids (Table 2). Moreover, fluorimetric displacement experiments with DP and DNSA revealed the association with binding site I because only the site I-selective ligand DNSA[34] is able to displace compound **3** from its binding pocket. Notably, the binding affinity of ligand **3** with BSA is much smaller than the ones with the nucleic acids, which is in line with the general observation that annelated quinolizinium derivatives are versatile and efficient DNA binders.[57]

The binding of ligand **3** with BSA was accompanied by the development of a strong fluorescence band at 627 nm. Like in the case of the association with the nucleic acids this light-up effect is likely caused by a suppressed formation of a CS or ICT excited state of the molecule within the binding site by a combination of restricted conformational freedom of the molecule and a lower polarity within the BSA binding pocket,[58] that has been estimated to have a medium polarity of $E^N_T = 0.21$.[59] The different polarity of the binding cavities of DNA[53] and BSA[58] may also be the reason for the blue-shifted emission of **3** in BSA ($\lambda_{fl} = 627$ nm) as compared with DNA and RNA ($\lambda_{Fl} = 725–750$ nm) because the CS or ICT state is stabilized more efficiently in the more polar DNA binding pocket than in the less polar BSA binding pocket. This assumption is in accordance with the relatively strong light-up effect in the presence of BSA ($\Phi_{fl} = 0.29$) as a result of a reduced formation of a CS or ICT state within the binding site.

3.4. Fluorimetric Analysis of Cells

In order to investigate the potential of ligand **3** to visualize cell components, NIH 3T3 mouse fibroblasts incubated with solutions of ligand **3** were examined by epifluorescence and confocal microscopy. Strong fluorescence in the cytoplasm was detected when ligand **3** was added to fixed cells. By contrast, this effect was missing in experiments, when living cells were incubated with a solution of ligand **3** and fixed afterwards just prior to microscopy. However, the paraformaldehyde fixative makes the lipid bilayer that builds the cell membrane porous[60] and therefore enables penetration into the cell, but not further into the nucleus. Although only a very weak epifluorescence was detected in the nucleus, the fluorescence signal exceeds 530 times the autofluorescence of the nucleus showing an ability of ligand **3** to permeate through the nuclear membrane, albeit with low efficiency. The nuclear membrane has different

characteristics than the outer cell membrane due to its higher cholesterol ratio.[61]

The fluorescence light-up effect of ligand **3** in NIH 3T3 mouse fibroblasts likely originates from the association with RNA and proteins in the cytoplasm and from the association with DNA and RNA in the nucleus, as supported by the same characteristic emission properties as the ones observed in fluorimetric titrations with the respective biomacromolecules (see above). Specifically, high fluorescence intensities were observed in the perinuclear region, where ribosomes, macromolecular structures consisting of proteins and RNA, are highly concentrated and where the overall thickness of the cell is also maximal compared to the cell periphery. Thus, the long fluorescence lifetime of the DNA- and (or) protein-bound ligand is likely indicative of the relatively high emission quantum yield. Complementary, the spatial variation of $<\tau>$ within the cell regions (Figure 8) might indicate a different binding efficiency of the ligand to the DNA, RNA and proteins or their distribution in the cell interior.[62] Finally, the emission detected with the filter set in the blue color range does not relate to the emission bands of the analyte-bound ligand at neutral conditions, but matches the emission of the protonated ligand instead (cf. Figure 2). Thus, it may be concluded that the blue emission indicates areas within the cell with relatively low pH, like the endolysosomal compartment, at which the ligand is partially protonated.[63]

4. Conclusion

In summary, a novel dimethylaminophenyl-substituted naphthoquinolizinium derivative was synthesized, which exhibits a high affinity towards several nucleic acids and induced a strong and selective stabilization of the quadruplex-forming oligonucleotides **22AG**, **c-kit** and **c-myc** and may thus be a promising starting point for the development of G4-DNA-targeting therapeutics.[64] Moreover, it was found that the ligand **3**, which is nearly non-fluorescent in aqueous buffer solution, exhibits a strong light-up effect in the presence of duplex and quadruplex DNA as well as RNA and BSA. The emission quantum yield is not very high, but at least sufficient to enable unambiguous signal detection, even with the naked eye. Moreover, the emission properties may be improved on demand in a next-generation probe because the quinolizinium fluorophore is easily modified for specific purposes.[18d] Most notably, the ligand exhibits a different fluorescence energy and intensity in the presence of BSA, as compared with those of all other tested biomacromolecules, which enables the fluorimetric differentiation between these analytes. Because of the strongly red-shifted NIR emission of derivative **3** upon complexation to all biomacromolecules it is a promising fluorescent probe for the analysis of biological systems in the more favorable NIR range.[2,3] To add to that, multicolor fluorescence was detected in the cytoplasm of NIH 3T3 mouse fibroblasts. Most interestingly, the various emission colors were distributed differently within the cytoplasm, and particularly the intensity of the emission in the blue-color range varied significantly, which enables the indication and visualization of cell areas with relatively low pH, like cellular compartments of the endolysosomal system. Furthermore, the varying fluorescence lifetimes of the probe when bound to macromolecules in the different environments in a cell may be utilized for the visualization of particular cell compartments, such as the nucleus and cytoplasm. For example, the ability of ligand **3** to differentiate between cell organelles may be investigated by future colocalization studies with known organelle markers.[1]

Experimental Section

Equipment

Absorption spectra: Varian Cary 100 Bio Spectrophotometer with baseline correction. Emission spectra: Varian Cary Eclipse spectrophotometer at 20 °C: Cuvettes: Quartz cells (10 mm × 4 mm). NMR spectra: Jeol ECZ 500 (^{1}H: 500 MHz, ^{13}C: 125 MHz) at 25 °C (DMSO-d_6). NMR spectra were processed with the software MestReNova and referenced to the residual solvent signals of DMSO-d_5 (^{1}H: δ = 2.50, ^{13}C: δ = 39.5). Elemental analyses data: HEKAtech EUROEA combustion analyser, by Rochus Breuer, Organische Chemie I, Universität Siegen. Mass spectra (ESI): Finnigan LCQ Deca (U = 6 kV; working gas: Ar; auxiliary gas: N_2; temperature of the capillary: 200 °C). Circular-dichroism (CD) and *flow*-linear-dichroism (LD) spectra: Chirascan CD spectrometer, Applied Photophysics. For LD spectra: High Shear Cuvette Cell Accessory (Applied Photophysics). The LD samples were recorded in a rotating cuvette with a shear gradient of 1200 s^{-1}. Melting points (uncorrected): BÜCHI 545 (BÜCHI, Flawil, CH). Epifluorescence microscopy for cell analysis was done with an Axiovert 135 microscope equipped with an AxioCamMRm and Zen 2.3lite software and the filter sets 49 (λ_{ex} = 320–390 nm, λ_{em} = 420–470 nm), 09 (λ_{ex} = 450–490 nm, λ_{em} > 515 nm), Lumar 15 (λ_{ex} = 540–552 nm, λ_{em} > 590 nm) from Carl Zeiss MicroImaging GmbH (Jena, Germany). The confocal fluorescence microscopy images and time-correlated single photon counting (TCSPC) data were measured at room temperature with a confocal laser scanning fluorescence microscope (PicoQuant, Berlin, Germany) composed of a Microtime 200 main optical unit, a FCU II fiber coupling unit, a PicoHarp 300 data acquisition module and an OLYMPUS IX-71 microscope frame (Olympus, Hamburg, Germany). Data were collected through an oil immersion 100x objective (UApo N100x/1.49 N.A., Olympus, Hamburg, Germany). Excitation wavelength was at 485 nm with a rate of 20 MHz by a LDH–D-C-485 pulsed laser (PicoQuant, Berlin, Germany) and fluorescence was detected with a PD1CTC Single-Photon Avalanche Diode detector (Micro Photon Devices, Bolzano, Italy) at a time resolution of 16 ps per channel. Images in the horizontal xy-plane were recorded with a piezo XYZ-scanner in an area of 80 × 80 μm^2 with 512 × 512 pixel resolution.

Materials

4-(*N*,*N*-Dimethylamino)phenylboronic acid (**6**),[65] and 3-bromonaphtho[1,2-*b*]quinolizinium bromide (**5**)[22] were synthesized according to published procedures. Calf thymus DNA (ct DNA, type I; highly polymerized sodium salt; ε = 12824 $cm^{-1}M^{-1}$)[66] and ty RNA (Ribonucleic acid, from torula yeast; ε = 8000 $cm^{-1}M^{-1}$)[67] were purchased from SigmaAldrich (St. Louis, USA) and used without further purification. Oligodeoxyribonucleotides (HPLC purified) d[A-($G_3TTA)_3G_3$] (**22AG**), d[($ACAG_4TGTG_4)_2$] (**a2**), d[$TGAG_3TG_3TAG_3TG_3TA$] (**cmyc**), d[($AG_3AG_3CGCTG_3AG_2AG_3$)] (**ckit**), d-($CA_2TCG_2ATCGA_2T_2CGATC2GAT_2G$] (**ds26**), d[fluo-$(GGGTAA)_3G_3$-tam-

ra] (**F21T**), d[fluo-$(ACAG_4TGTG_4)_2$-tamra] (**Fa2T**), d[fluo-$TGAG_3TG_3TAG_3TG_3TA$-tamra] (**FmycT**) and d[fluo-$(AG_3AG_3CGCTG_3AG_2AG_3)$-tamra] (**FkitT**) (fluo = fluorescein, tamra = tetramethylrhodamine) were purchased from Metabion Int. AG (Planegg/Martinsried). BSA was purchased from Acros Organics (Pittsburgh, USA). The concentration of ct DNA is given in base pairs (bp), the concentration of ty RNA is given in bases and the concentrations of oligonucleotides are given in oligonucleotides.

The ct DNA was dissolved in BPE buffer solution. RNA solutions were prepared in TBS buffer. Solutions of oligonucleotides were prepared in K-phosphate buffer (pH 7), heated to 95 °C for 5 min and cooled slowly to room temperature within 4 h. Britton-Robinson-buffer: 40 mM H_3PO_4, 40 mM H_3BO_3, 40 mM NaOAc; K-phosphate buffer: 25 mM K_2HPO_4, 70 mM KCl; adjusted with 50 mM KH_2PO_4, 70 mM KCl to pH 7.0; BPE (biphosphate EDTA) buffer: 6.0 mM Na_2HPO_4, 2.0 mM NaH_2PO_4, 1.0 mM Na_2EDTA; pH 7.0; TBS: 50 mM TRIS, 150 mM NaCl; pH 7.0. All buffer solutions were prepared from purified water (resistivity 18 MΩ cm) and biochemistry-grade chemicals. The buffer solutions were filtered through a PVDF membrane filter (pore size 0.45 μm) prior to use.

Synthesis

3-(4-(N,N-Dimethylamino)phenyl)naphtho[1,2-b]quinolizinium (**3**). A mixture of 3-bromonaphtho[1,2-*b*]quinolizinium bromide (**5**) (195 mg, 500 μmol), 4-(*N,N*-dimethylaminophenyl)boronic acid (**6**) (90.8 mg, 550 μmol), Pd(dppf)Cl_2·CH_2Cl_2 (12.3 mg) and KF (116 mg, 2.00 mmol) in DME/water/MeOH (2 : 1 : 1, 8 ml) was stirred for 2 h at 80 °C under argon gas atmosphere. After cooling to r.t. the resulting precipitate was separated by filtration and washed with DME/water/MeOH (5 ml) and EtOAc (3 × 10 ml). The crude product was purified by column chromatography (SiO_2, CH_2Cl_2/MeOH 95 : 5 → 91 : 9; R_f = 0.45 at CH_2Cl_2/MeOH 91 : 9) to afford **3** as red amorphous solid (155 mg, 361 μmol, 72 %); mp > 300 °C (dec.). – ^{1}H NMR (500 MHz, DMSO-d_6): δ = 3.01 (s, 6H, NCH_3), 6.86 (d, ^3J = 9 Hz, 2H, 2′-H, 6′-H), 7.82 (d, ^3J = 9 Hz, 2H, 3′-H, 5′-H), 8.00 (t, ^3J = 7 Hz, 1H, 10-H), 8.08 (d, ^3J = 9 Hz, 1H, 6-H), 8.21 (m, 1H, 11-H), 8.22 (m, 1H, 5-H), 8.23 (m, 2 H, 2-H), 8.39 (s, 1 H, 4-H), 8.60 (d, ^3J = 8 Hz, 1H, 12-H), 9.04 (d, ^3J = 9 Hz, 1H, 1-H), 9.32 (d, ^3J = 7 Hz, 1 H, 9-H), 9.95 (s, 1H, 13-H), 10.19 (s, 1H, 7-H). – ^{13}C NMR (125 MHz, DMSO-d_6): δ = 39.8 (NCH_3) 112.5 (C2′, C6′), 119.8 (C13), 122.4 (C10), 123.5 (C6), 124.4 (C13b), 124.9 (C4), 125.2 (C4′), 125.6 (C6a), 125.8 (C1), 126.3 (C2), 126.8 (C12), 127.8 (C3′, C5′), 132.8 (C11), 133.0 (C5), 134.3 (C4a), 134.6 (C9), 135.4 (C13a), 137.3 (C7), 138.9 (C12a), 143.3 (C3), 150.6 (C1′). – MS (ESI^+): *m/z* = 349 $[M–Br]^+$. – El. Anal. for $C_{25}H_{21}BrN_2$ x H_2O, calc. (%): C 67.12, H 5.18, N 6.26, found (%): C 66.75, H 4.91, N 5.89.

Eukaryotic Cells Culture and Fluorescent Staining of Cells

NIH 3T3 mouse fibroblasts7 were cultured at standard conditions like previously described[18a] and fixed at around 70 % confluency, washed gently three times with prewarmed (37 °C) PBS (Lonza, Belgium) and fixed with 4 % paraformaldehyde in PBS for 20 min at 21 °C before fluorescent labeling with **3** (5 μM) in PBS that had been prepared as stock solution of 2 mM **3** in DMSO. In case the fluorescent labeling with **3** was performed with living cells, the culture medium was removed and prewarmed culture media with 2.5 μM **3** was added. As controls, cells have been in parallel incubated with cell culture media or PBS only with the same final concentration of 0.25 % (v/v) DMSO.

After staining of living cells they were washed two times with prewarmed (37 °C) PBS and the fixation protocol was performed as described above. Before final sample embedding with Mowiol® 4–88 (Carl Roth) samples were washed three times with PBS and were washed once via dipping in Milli-Q water.

Acknowledgements

Generous support by the Deutsche Forschungsgemeinschaft (Ih24/14-1, Ih24/17-1, Scho1124/7-1, INST221-87/1 FUGG), ERASMUS program (Manlio Sutera Sardo), and the University of Siegen is gratefully acknowledged. We thank Dr. Daria Berdnikova and Dipl.-Biol. Sabine Wenderhold-Reeb for technical assistance, Christoph Dohmen for photographic documentation, and Dr. Jürgen Schnekenburger (Biomedical Technology Center of Medical Faculty, Münster, Germany), who kindly provided the NIH 3T3 cell line. Open Access funding enabled and organized by Projekt DEAL.

Conflict of Interest

The authors declare no conflict of interest.

Keywords: bioorganic chemistry · cell imaging · fluorescent probes · intercalation · nucleic acids

[1] a) A. Saini, J. Singha, S. Kumar, *Org. Biomol. Chem.* **2021**, *19*, 5208–5236; b) J.-F. Wang, C.-M. Zhao, J.-X. Yang, X. He, X.-L. Li, J.-M. Li, K.-R. Wang, *Chem. Commun.* **2021**, *57*, 2776–2779; c) N.-E. Choi, J.-Y. Lee, E.-C. Park, J.-H. Lee, J. Lee, *Molecules* **2021**, *26*, 217; d) T. Yang, A. Chettri, B. Radwan, E. Matuszyk, M. Baranska, B. Dietzek, *Chem. Commun.* **2021**, *57*, 6392–6395; e) V. P. Jejurkar, G. Yashwantrao, P. Kumar, S. Neekhra, P. J. Maliekal, P. Badani, R. Srivastava, S. Saha, *Chem. Eur. J.* **2021**, *27*, 5470–5482; f) Y. Bai, W. Wan, Y. Huang, W. Jin, H. Lyu, Q. Xia, X. Dong, Z. Gaoc, Y. Liu, *Chem. Sci.* **2021**, *12*, 8468–8476; g) X. Tian, L. C. Murfin, L. Wu, S. E. Lewis, T. D. James, *Chem. Sci.* **2021**, *12*, 3406–3426; h) L. George, F. E. Indig, K. Abdelmohsen, M. Gorospe, *Open Biol.* **2018**, *8*, 180104.
[2] S. Wang, B. Li, F. Zhang, *ACS Cent. Sci.* **2020**, *6*, 1302–1316.
[3] B. Li, M. Zhao, F. Zhang, *ACS Materials Lett.* **2020**, *2*, 905–917.
[4] A. K. Das, H. Ihmels, S. Kölsch, *Photochem. Photobiol. Sci.* **2019**, *18*, 1373–1381.
[5] R. Bortolozzi, H. Ihmels, L. Thomas, M. Tian, G. Viola, *Chem. Eur. J.* **2013**, *19*, 8736–8741.
[6] F. Wu, C. Liu, Y. Chen, S. Yang, J. Xu, R. Huang, X. Wang, M. Li, W. Liu, W. Mao, X. Zhou, *Sens. Actuator. B Chem.* **2016**, *236*, 268–275.
[7] B. Kumari, A. Yadav, S. P. Pany, P. I. Pradeepkumar, S. Kanvah, *J. Photochem. Photobiol. B* **2019**, *190*, 128–136.
[8] L.-Y. Liu, W. Liu, K.-N. Wang, B.-C. Zhu, X.-Y. Xia, L.-N. Ji, Z.-W. Mao, *Angew. Chem. Int. Ed.* **2020**, *59*, 9719–9726; *Angew. Chem.* **2020**, *132*, 9806–9813.
[9] K.-N. Wang, Q. Cao, L.-Y. Liu, Z.-J. Zhao, W. Liu, D.-J. Zhou, C.-P. Tan, W. Xia, L.-N. Ji, Z.-W. Mao, *Chem. Sci.* **2019**, *10*, 10053–10064.
[10] I. E. H. Elhussin, S. Zhang, J. Liu, D. Li, Q. Zhang, S. Li, X. Tian, J. Wu, Y. Tian, *Chem. Commun.* **2020**, *56*, 1859–1862.
[11] a) I. Gaspar, F. Hövelmann, J. Chamiolo, A. Ephrussi, O. Seitz, *ACS Chem. Biol.* **2018**, *13*, 742–749; b) H. Wu, S. C. Alexander, S. Jin, N. K. Devaraj, *J. Am. Chem. Soc.* **2016**, *138*, 11429–11432.
[12] S. I. Reja, M. Minoshima, Y. Hori, K. Kikuchi, *Chem. Sci.* **2021**, *12*, 3437–3447.
[13] X. Feng, A. Sureda, S. Jafari, Z. Memariani, D. Tewari, G. Annunziata, L. Barrea, S. T. S. Hassan, K. Šmejkal, M. Malaník, A. Sychrová, D. Barreca, L. Ziberna, M. F. Mahomoodally, G. Zengin, S. Xu, S. M. Nabavi, A.-Z. Shen, *Theranostics* **2019**, 1923–1951.
[14] P. M. Pithan, D. Decker, S. I. Druzhinin, H. Ihmels, H. Schönherr, Y. Voß, *RSC Adv.* **2017**, *7*, 10660–10667.

[15] M.-H. Hu, *Anal. Chim. Acta* **2021**, *1169*, p. 338600.
[16] L.-L. Li, H.-R. Xu, K. Li, Q. Yang, S.-L. Pan, X.-Q. Yu, *Sens. Actuator. B Chem.* **2019**, *286*, 575–582.
[17] V. Grande, F. Doria, M. Freccero, F. Würthner, *Angew. Chem. Int. Ed.* **2017**, *56*, 7520–7524; *Angew. Chem.* **2017**, *129*, 7628–7632.
[18] a) A. K. Das, S. I. Druzhinin, H. Ihmels, M. Müller, H. Schönherr, *Chem. Eur. J.* **2019**, *25*, 12703–12707; b) F. Li, J. Cho, S. Tan, S. Kim, *Org. Lett.* **2018**, *20*, 824–827; c) E. Zacharioudakis, T. Cañeque, R. Custodio, S. Müller, A. M. Cuadro, J. J. Vaquero, R. Rodriguez, *Bioorg. Med. Chem. Lett.* **2017**, *27*, 203–207; d) A. Granzhan, H. Ihmels, M. Tian, *Arkivoc* **2015**, *vi*, 494–523; e) X. Yue, Z. Armijo, K. King, M. V. Bondar, A. R. Morales, A. Frazer, I. A. Mikhailov, O. V. Przhonska, K. D. Belfield, *ACS Appl. Mater. Interfaces* **2015**, *7*, 2833–2846; f) G. Marcelo, S. Pinto, T. Cañeque, I. F. A. Mariz, A. M. Cuadro, J. J. Vaquero, J. M. G. Martinho, E. M. S. Maçôas, *J. Phys. Chem. A* **2015**, *119*, 2351–2362; g) K. Faulhaber, A. Granzhan, H. Ihmels, D. Otto, L. Thomas, S. Wells, *Photochem. Photobiol. Sci.* **2011**, *10*, 1535–1545.
[19] H. Ihmels, K. Faulhaber, C. Sturm, G. Bringmann, K. Messer, N. Gabellini, D. Vedaldi, G. Viola, *Photochem. Photobiol.* **2001**, *74*, 505–511.
[20] G. Viola, M. Bressanini, N. Gabellini, D. Vedaldi, F. Dall'Acqua, H. Ihmels, *Photochem. Photobiol. Sci.* **2002**, *1*, 882–889.
[21] a) A. Barbafina, M. Amelia, L. Latterini, G. G. Aloisi, F. Elisei, *J. Phys. Chem. A* **2009**, *113*, 14514–14520; b) H. Ihmels, C. J. Mohrschladt, A. Schmitt, M. Bressanini, D. Leusser, D. Stalke, *Eur. J. Org. Chem.* **2002**, 2624–2632.
[22] P. M. Pithan, D. Decker, M. S. Sardo, G. Viola, H. Ihmels, *Beilstein J. Org. Chem.* **2016**, *12*, 854–862.
[23] M. Tian, H. Ihmels, *Synthesis* **2009**, *24*, 4226–4234.
[24] A. Bax, M. F. Summers, *J. Am. Chem. Soc.* **1986**, *108*, 2093–2094.
[25] G. Oster, Y. Nishijima, *J. Am. Chem. Soc.* **1956**, *78*, 1581–1584.
[26] L. Andrussow, B. Schramm, K. Schäfer (Eds.) *Eigenschaften der Materie in ihren Aggregatzuständen. Transportphänomene I (Viskosität und Diffusion)*, Springer, Berlin, **1969**.
[27] H. Elias, *Ber. Bunsenges. Phys. Chem.* **1990**, *94*, 537–538.
[28] X.-F. Zhang, Y. Zhang, L. Liu, *J. Lumin.* **2014**, *145*, 448–453.
[29] D. Rhodes, H. J. Lipps, *Nucleic Acids Res.* **2015**, *43*, 8627–8637.
[30] B. Gatto, M. Palumbo, C. Sissi, *Curr. Med. Chem.* **2009**, *16*, 1248–1265.
[31] R. I. Mathad, E. Hatzakis, J. Dai, D. Yang, *Nucleic Acids Res.* **2011**, *39*, 9023–9033.
[32] S. Rankin, A. P. Reszka, J. Huppert, M. Zloh, G. N. Parkinson, A. K. Todd, S. Ladame, S. Balasubramanian, S. Neidle, *J. Am. Chem. Soc.* **2005**, *127*, 10584–10589.
[33] A. de Cian, L. Guittat, M. Kaiser, B. Saccà, S. Amrane, A. Bourdoncle, P. Alberti, M.-P. Teulade-Fichou, L. Lacroix, J.-L. Mergny, *Methods* **2007**, *42*, 183–195.
[34] V. S. Jisha, K. T. Arun, M. Hariharan, D. Ramaiah, *J. Phys. Chem. B* **2010**, *114*, 5912–5919.
[35] F. H. Stootman, D. M. Fisher, A. Rodger, J. R. Aldrich-Wright, *Analyst* **2006**, *131*, 1145–1151.
[36] J. L. Jainchill, S. A. Aaronson, G. L. Todaro, *J. Virol.* **1969**, *4*, 549–553.
[37] Z. R. Grabowski, K. Rotkiewicz, W. Rettig, *Chem. Rev.* **2003**, *103*, 3899–4032.
[38] N. Mataga, Y. Kaifu, M. Koizumi, *Bull. Chem. Soc. Jpn.* **1956**, *29*, 465–470.
[39] a) S. I. Druzhinin, S. R. Dubbaka, P. Knochel, S. A. Kovalenko, P. Mayer, T. Senyushkina, K. A. Zachariasse, *J. Phys. Chem. A* **2008**, *112*, 2749–2761; b) S. I. Druzhinin, N. P. Ernsting, S. A. Kovalenko, L. P. Lustres, T. A. Senyushkina, K. A. Zachariasse, *J. Phys. Chem. A.* **2006**, *110*, 2955–2969; c) K. A. Zachariasse, S. I. Druzhinin, W. Bosch, R. Machinek, *J. Am. Chem. Soc.* **2004**, *126*, 1705–1715.
[40] a) W. Rettig, V. Kharlanov, M. Maus, *Chem. Phys. Lett.* **2000**, *318*, 173–180; b) V. Kharlanov, W. Rettig, *Chem. Phys.* **2007**, *332*, 17–26.
[41] a) T. Förster, G. Hoffmann, *Z. physik. Chem.* **1971**, *75*, 63–76; b) M. Belletête, R. S. Sarpal, G. Durocher, *Chem. Phys. Lett.* **1993**, *201*, 145–152.
[42] S. I. Druzhinin, V. A. Galievsky, T. Yoshihara, K. A. Zachariasse, *J. Phys. Chem. A* **2006**, *110*, 12760–12768.
[43] S. Yalcin, L. Thomas, M. Tian, N. Seferoglu, H. Ihmels, Y. Dede, *J. Org. Chem.* **2014**, *79*, 3799–3808.
[44] a) D. Dzubiel, H. Ihmels, M. M. A. Mahmoud, L. Thomas, *Beilstein J. Org. Chem.* **2014**, *10*, 2963–2974; b) J. Becher, D. V. Berdnikova, H. Ihmels, C. Stremmel, *Beilstein J. Org. Chem.* **2020**, *16*, 2795–2806; c) P. J. Wickhorst, H. Ihmels, *Chem. Eur. J.* **2021**, *27*, 8580–8589.
[45] B. Nordén, A. Rodger, T. Dafforn, *Linear dichroism and circular dichroism. A textbook on polarized-light spectroscopy*, RSC Publ, Cambridge, **2010**.
[46] T. Šmidlehner, I. Piantanida, G. Pescitelli, *Beilstein J. Org. Chem.* **2018**, *14*, 84–105.
[47] B. Nordén, T. Kurucsev, *J. Mol. Recognit.* **1994**, *7*, 141–155.
[48] a) S. Geisler, J. Coller, *Nat. Rev. Mol. Cell Biol.* **2013**, *14*, 699–712; b) S. Zehra, T. Roisnel, F. Arjmand, *ACS Omega* **2019**, *4*, 7691–7705.
[49] H. Ihmels, M. M. A. Mahmoud, B. O. Patrick, *J. Phys. Org. Chem.* **2017**, *30*, e3736.
[50] a) D. Renciuk, I. Kejnovská, P. Skoláková, K. Bednárová, J. Motlová, M. Vorlícková, *Nucleic Acids Res.* **2009**, *37*, 6625–6634; b) A. Ambrus, D. Chen, J. Dai, T. Bialis, R. A. Jones, D. Yang, *Nucleic Acids Res.* **2006**, *34*, 2723–2735.
[51] A. K. Jain, S. Bhattacharya, *Bioconjugate Chem.* **2011**, *22*, 2355–2368.
[52] a) T. Yamashita, T. Uno, Y. Ishikawa, *Bioorg. Med. Chem.* **2005**, *13*, 2423–2430; b) H. Sun, Y. Tang, J. Xiang, G. Xu, Y. Zhang, H. Zhang, L. Xu, *Bioorg. Med. Chem. Lett.* **2006**, *16*, 3586–3589.
[53] A. Cuervo, P. D. Dans, J. L. Carrascosa, M. Orozco, G. Gomila, L. Fumagalli, *Proc. Natl. Acad. Sci. USA* **2014**, *111*, E3624–3630.
[54] a) P. Catasti, X. Chen, R. K. Moyzis, E. M. Bradbury, G. Gupta, *J. Mol. Biol.* **1996**, *264*, 534–545; b) L. Xu, S. Hong, N. Sun, K. Wang, L. Zhou, L. Ji, R. Pei, *Chem. Commun.* **2016**, *52*, 179–182.
[55] a) A. T. Phan, V. Kuryavyi, S. Burge, S. Neidle, D. J. Patel, *J. Am. Chem. Soc.* **2007**, *129*, 4386–4392; b) S. Stump, T.-C. Mou, S. R. Sprang, N. R. Natale, H. D. Beall, *PLoS One* **2018**, *13*, e0205584.
[56] H. Ihmels, D. Otto, F. Dall'Acqua, A. Faccio, S. Moro, G. Viola, *J. Org. Chem.* **2006**, *71*, 8401–8411.
[57] A. Granzhan, H. Ihmels, *Synlett* **2016**, *27*, 1775–1793.
[58] J. Eden, P. R. C. Gascoyne, R. Pethig, *J. Chem. Soc. Faraday Trans. 1* **1980**, *76*, 426–434.
[59] S. Ercelen, A. S. Klymchenko, A. P. Demchenko, *FEBS Lett.* **2003**, *538*, 25–28.
[60] M. C. Jamur, C. Oliver, *Methods Mol. Biol.* **2010**, *588*, 63–66.
[61] M. Garnier-Lhomme, R. D. Byrne, T. M. C. Hobday, S. Gschmeissner, R. Woscholski, D. L. Poccia, E. J. Dufourc, B. Larijani, *PLoS One* **2009**, *4*, e4255.
[62] J. M. O'Sullivan, D. A. Pai, A. G. Cridge, D. R. Engelke, A. R. D. Ganley, *Biomol. Concepts* **2013**, *4*, 277–286.
[63] G. M. Cooper (Ed.) *The Cell: A Molecular Approach. 2nd edition*, Sinauer Associates, **2000**.
[64] a) S. Neidle, *J. Med. Chem.* **2016**, *59*, 5987–6011; b) D. Rhodes, H. J. Lipps, *Nucleic Res.* **2015**, *43*, 8627–8637.
[65] D. Oesch, N. W. Luedtke, *Chem. Commun.* **2015**, *51*, 12641–12644.
[66] J. Ren, J. B. Chaires, *Biochemistry* **1999**, *38*, 16067–16075.
[67] J. Steyaert, C. Opsomer, L. Wyns, P. Stanssens, *Biochemistry* **1991**, *30*, 494–499.

Manuscript received: July 15, 2021
Revised manuscript received: August 26, 2021
Accepted manuscript online: August 29, 2021
Version of record online: ■■, ■■■

ARTICLES

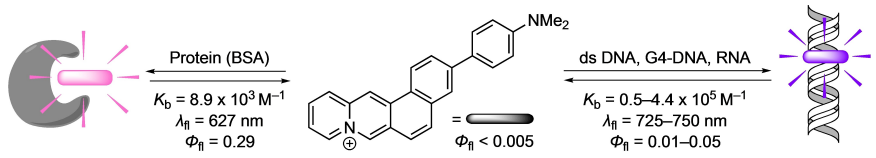

Light up, light up: The fluorimetric detection of different biomacromolecules is accomplished with 3-(4-*N*,*N*-dimethylaminophenylnaphtho[1,2-*b*]-quinolizinium as a fluorescent probe. This molecule shows a light-up effect in the presence of DNA, RNA and bovine serum albumin (BSA) with different emission energies, intensities, and lifetimes. These effects may be used for the fluorimetric differentiation between different cell compartments.